Ma et al. *NPG Asia Materials* (2020) 12:70
https://doi.org/10.1038/s41427-020-00251-2

NPG Asia Materials

ARTICLE Open Access

Flexible transparent heteroepitaxial conducting oxide with mobility exceeding 100 $cm^2 V^{-1} s^{-1}$ at room temperature

Chun-Hao Ma[1], En-Liang Chen[1], Yu-Hong Lai[1], Yi-Cheng Chen[1], Li Chang[1] and Ying-Hao Chu[1,2]

Abstract

Flexible and transparent applications have become an emerging technology and have shifted to the forefront of materials science research in recent years. Transparent conductive oxide films have been applied for flat panel displays, solar cells, and transparent glass coatings. However, none of them can fulfill the requirements for advanced transparent flexible devices, such as high-frequency applications. Here, we present a promising technique for transparent flexible conducting oxide heteroepitaxial films: the direct fabrication of epitaxial molybdenum-doped indium oxide (IMO) thin films on a transparent flexible muscovite substrate. An n-type epitaxial IMO film is demonstrated with a mobility of 109 $cm^2 V^{-1} s^{-1}$, a figure of merit of 0.0976 Ω^{-1}, a resistivity of 4.5×10^{-5} Ω cm and an average optical transmittance of 81.8% in the visible regime. This heteroepitaxial system not only exhibits excellent electrical and optical performance but also shows excellent mechanical durability. Our results illustrate that this is an outstanding way to fabricate transparent and flexible conducting elements for the evolution and expansion of next-generation smart devices.

Introduction

Transparent conductive oxides (TCOs) exhibit impressive properties, including excellent electrical conductivity and high optical transmittance in the visible light range[1,2]. They have attracted great interest due to their potentially disruptive application in optoelectronics, including flat panel displays, light-emitting diodes, thin-film transistors, solar cells and a variety of other applications that use both their electronic and transmittance features[3–6]. With their dramatically advanced properties for the integration of additional functionalities, flexible electronics- and numerous-related applications have become important research directions for soft technologies and wearable electronics[7,8]. In this research field, transparent flexible conducting components with excellent performance play a key role in almost all optoelectronics. Thus, the development of high-quality transparent flexible conducting elements has attracted a substantial amount of attention and become a promising research direction for next-generation consumer electronics.

Among the well-known TCOs, indium tin oxide (ITO) is the most extensively studied and widely used in light-emitting diodes, liquid crystal displays, and photovoltaic applications, for example[9,10]. ITO exhibits the desirable combination of a high electrical conductivity and high optical transparency. High-quality epitaxial ITO thin films possess a low resistivity of 2.3×10^{-4} Ω cm with a carrier concentration of 4.8×10^{20} cm^{-3} and mobility of 56 $cm^2 V^{-1} s^{-1}$[11]. However, the characteristics of ITO films are still not acceptable enough to fulfill the requirements for advanced optoelectronics, especially thin-film transistors, thin-film solar cells and high-frequency devices, due to their requirements of a super high charge mobility for improving their performance. For instance, in the study of

Correspondence: Ying-Hao Chu (yhc@nctu.edu.tw)
[1]Department of Materials Science and Engineering, National Chiao Tung University, 30010 Hsinchu, Taiwan
[2]Center for Emergent Functional Matter Science, National Chiao Tung University, 30010 Hsinchu, Taiwan

optically transparent patch antennas, a large enhancement in the microstrip efficiency with resonant frequencies between 100 MHz and 10 GHz was obtained with an increase in the electron mobility from 50 $cm^2 V^{-1} s^{-1}$ to 100 $cm^2 V^{-1} s^{-1}$[12]. Moreover, even with a high crystalline quality, the mobility of ITO is reduced for films fabricated on flexible substrates[13,14]. Therefore, it is productive to search for new candidates that break this barrier.

The large room-temperature mobility of molybdenum-doped indium oxide (IMO) films coupled with a low resistivity, high carrier concentration and optical transparency makes them a candidate for transparent flexible conducting elements to replace ITO films[15,16]. An IMO film was reported to show a resistivity of $1.7 \times 10^{-4}\ \Omega$ cm, a mobility over 100 $cm^2 V^{-1} s^{-1}$ and an average optical transmittance over 80% in the visible range[17]. Because molybdenum ions have a low affinity for oxygen ions and do not incorporate excess oxygen ions in their lattice, doped molybdenum can reduce the scattering centers, resulting in high-mobility IMO. In addition, when the valence difference between the dopant and substituted ion is 3, TCO can have a high carrier concentration, as shown by these defect chemical equations:

$$In_{In} + Mo\,O_3 \rightarrow Mo_{In}^{\cdots} + 1/2\,In_2\,O_3 + 3/4\,O_2 + 3e^-$$

$$Mo_{In}^{\cdots} O^{2-} \rightarrow Mo_{In}^{\cdots} + 1/2O_2 + 2e^-$$

$$O_O \rightarrow 1/2O_2 + V_O^{\cdot\cdot} + 2e^-$$

Both a high-mobility and high carrier concentration make IMO an extraordinary TCO with excellent performance. Therefore, it is worth considering the challenges and fabricating transparent flexible conducting IMO thin films for advanced transparent flexible applications.

To produce a high-mobility conducting element featuring optical transparency as well as mechanical flexibility, two necessary components must be combined. (1) There must be a high-quality epitaxial IMO thin film with low resistivity, high-mobility and high carrier concentration. (2) There must be an ideal substrate with a crystalline structure, high optical transparency and robustness against mechanical constraints. Recently, muscovite mica has been studied and identified as a favorable transparent flexible substrate for heteroepitaxial oxide films[18,19]. Numerous high-quality flexible oxide heterostructures were demonstrated that had excellent performance, providing new candidates for flexible applications. In this work, we demonstrate the fabrication of a high-mobility transparent flexible conducting heterostructure composed of heteroepitaxial IMO/mica. In our study, the heteroepitaxial IMO/mica system not only exhibits high electron conductivity and high optical transparency but also shows excellent stability against mechanical bending. Our results achieve an important step in the evolution of progressive optoelectronics.

Materials and methods

Growth of the IMO/AZO/mica Heterostructure

The epitaxial IMO/AZO/mica heterostructure was deposited via RF magnetron sputtering using commercial IMO (96% In_2O_3 and 4% MoO_3) and AZO (98% ZnO and 2% Al_2O_3) targets with a diameter of 3 inches. An exfoliated artificial muscovite mica (1 × 1 cm) without treatment was used in this study. The vacuum chamber was pumped to a base pressure of 10^{-6} Torr prior to deposition. During growth of the IMO and AZO, the chamber was maintained at 3 mTorr with an Ar flow of 20 sccm and an oxygen flow of 0.1 sccm. The deposition processes for both IMO and AZO were conducted while the substrate was heated to 550 °C, and the RF power was 100 W. After deposition, the heterostructures were annealed in situ at 750 °C for 1 h in the same atmosphere as during growth to improve the electrical conductivity.

Structural analysis

X-ray diffraction (XRD) $\theta-2\theta$ scans along the normal direction and Φ scans were performed to obtain structural information in a Bruker D8 high-resolution X-ray diffractometer using a monochromatic Cu $K_{\alpha 1}$ radiation source. Cross-sectional TEM was used to study the microstructure of the heterostructure. The TEM specimens were prepared by a focused ion beam system along the normal direction. X-ray photoelectron spectroscopy spectra were obtained in a ULVAC-PHI PHI 5000 Versaprobe II.

Conductivity and transparency properties

The resistivity and Hall measurements were conducted in a physical property measurement system. The optical transmittance spectra were gathered in a PerkinElmer Lambda-900 spectrometer.

Bending tests

A homebuilt computer-controlled bending system was used to conduct all bending tests. While one end was fixed, the other end could be moved by a stepping motor. The heterostructure was bent by the bending system and observed by an additional microscope.

Results and discussion

In this study, epitaxial IMO thin films were grown on muscovite by RF sputtering. The crystal structure and phase identification of the heteroepitaxial films were then characterized by XRD. Moreover, as shown in Fig. 1a, an Al-doped ZnO (AZO) layer was inserted between the IMO and mica as a seed layer to enable the epitaxial growth of a high-quality IMO film. It is difficult to deposit

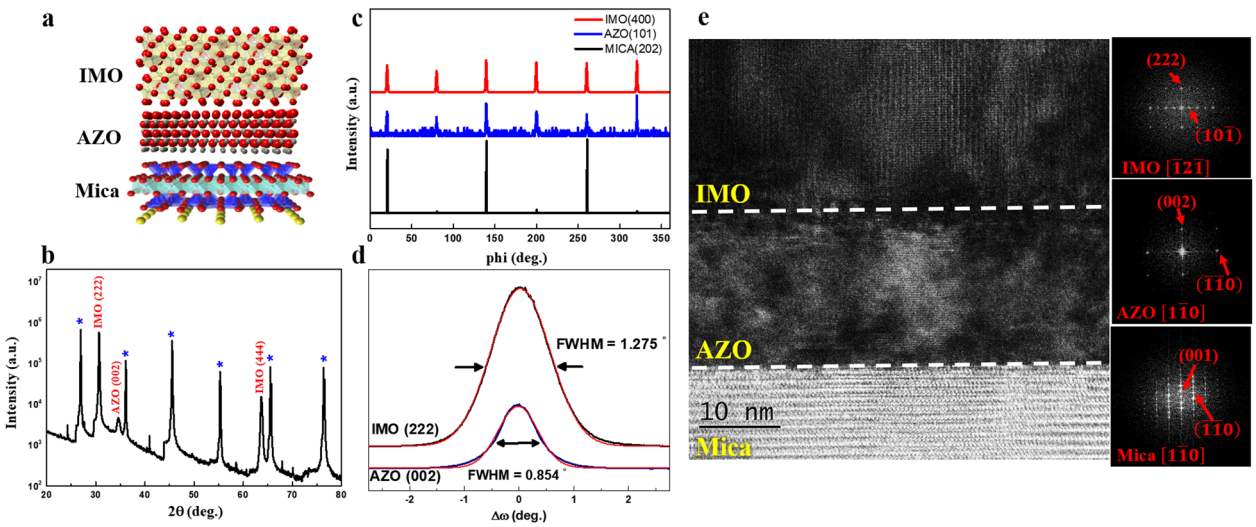

Fig. 1 IMO–AZO–mica heteroepitaxial structure. a Schematic of the IMO/AZO/mica heterostructure. **b** Typical θ–2θ scan of the heterostructure. **c** Φ-scans for IMO{400}, AZO {101}, and muscovite {202} diffraction peaks. **d** Rocking curves for IMO (222) and AZO (002) diffraction peaks. **e** Cross-sectional TEM image of the IMO/AZO/mica interface and fast Fourier transform images for the IMO, AZO, and mica.

an epitaxial IMO thin film on bare muscovite without a seed layer since the surface energies of IMO are similar for different orientations. Figure 1b shows an out-of-plane θ−2θ scan of the IMO/AZO/mica heteroepitaxial system. Only IMO (*lll*), AZO (*00l*) and muscovite (*00l*) diffraction peaks can be observed, indicating epitaxy of the heterostructure without undesirable secondary phases. The out-of-plane d-spacing of the IMO (222) planes was calculated from the XRD peak position and was 2.912 Å, suggesting a slight compressive strain of 0.3%. This measured strain was caused by the defects created during the deposition process and not the interaction between the IMO and muscovite substrate attributed to the van der Waals epitaxy. Moreover, Φ scans of IMO, AZO and muscovite reflections were applied to identify the in-plane epitaxial relationships, as shown in Fig. 1c. A primary set and two secondary sets of muscovite peaks at 120° intervals with different intensities suggest that different stacking sequences existed in the muscovite. Cubic bixbyite ITO {400} and hexagonal AZO {101} exhibited six peaks at 60° intervals, which indicates the existence of multidomain IMO and single crystalline AZO films on the muscovite substrate. Based on the XRD results, the epitaxial relationship was determined to be $(111)_{IMO}//(001)_{AZO}//(001)_{mica}$ and $(01–1)_{IMO}//(010)_{AZO}//(010)_{mica}$ for the IMO/AZO/mica heterostructure. To gather critical information about the crystallinity, rocking curve measurements were carried out, and the full width at half maximum values of ~1.28° and ~0.85° were determined for the IMO (222) and AZO (002) peaks, respectively, as shown in Fig. 1d. Furthermore, to study the microstructure of the IMO/AZO/mica heterostructure as well as explore the heteroepitaxy, interfaces between the thin films and substrate were investigated by transmission electron microscopy (TEM). Figure 1e exhibits high-resolution cross-sectional TEM images captured along the $[010]_{mica}$ direction, showing clear and defect-free IMO/AZO/mica interfaces. The reciprocal lattices of the IMO, AZO and muscovite, obtained from fast Fourier transforms, were clearly indexed to distinguish the structural information regarding the IMO/AZO/mica heteroepitaxy. The consistency of the epitaxial relationships between XRD and TEM results was carefully confirmed. The clear interfaces without observable defects indicate the presence of good heteroepitaxy. From the XRD and TEM results, high-quality IMO/AZO/mica heteroepitaxy was fabricated, which is key to attaining excellent properties. To verify the valence state of the In and Mo ions in the heterostructure and confirm the chemical composition, X-ray photoelectron spectroscopy (XPS) measurements were carried out. As shown in Supplementary Fig. 1, a typical XPS spectrum was obtained from the surface of the IMO/AZO/mica heterostructure. The high-resolution spectra of the In 3d and Mo 3d core levels indicate that the valence state of In was +3 and that for Mo was +6 in the heterostructure. By analyzing the XPS spectrum, the ratio of Mo dopant can be confirmed as ~4 wt % in the IMO films. It has been reported that IMO thin films exhibit a relatively high electron mobility as well as low resistivity at this doping level[17,20–22].

After the production of van der Waals epitaxy in the IMO/AZO/mica heterostructure, it is crucial to build a comprehensive and quantitative knowledge of the characteristics of this heteroepitaxy for advanced soft

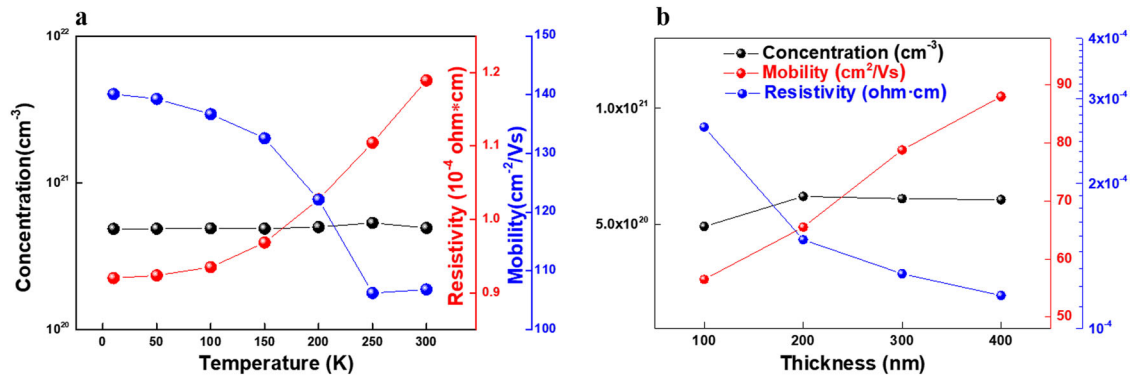

Fig. 2 Conducting behavior of the IMO/AZO/mica heterostructure. a Variations in the resistivity, concentration, and mobility as a function of temperature; and **b** the thickness dependence of the resistivity, concentration and mobility of the IMO film.

electronics. Electrical contacts were fabricated in the van der Pauw configuration. Temperature-dependent Hall measurements were carried out to characterize the charge carrier type and carrier concentration of the IMO heteroepitaxial structure. The resistivity, mobility and carrier concentration as a function of temperature of the heterostructure are shown in Fig. 2a. The IMO/AZO/mica heterostructure exhibited excellent conductivity ($\rho < 1.2 \times 10^{-4}\,\Omega$ cm) with a high mobility ($\mu = 109\,cm^2\,V^{-1}\,s^{-1}$) at room temperature. The resistivity decreased with temperature across the whole temperature range, exhibiting nearly metallic behavior. In addition, this behavior can be simply controlled by annealing the samples in different oxygen atmospheres. The IMO heteroepitaxial structure, annealed in a high oxygen pressure, exhibited insulating behavior and its resistivity increased as the temperature increased, as shown in Supplementary Fig. S2. The Hall measurement of the heterostructure confirmed the n-type conducting nature. The carrier concentration, n, was $1.27 \times 10^{21}\,cm^{-3}$ and showed almost no temperature dependence. The Hall electron mobility reached a value of $109\,cm^2\,V^{-1}\,s^{-1}$ at 300 K and $140\,cm^2\,V^{-1}\,s^{-1}$ at 10 K. The thickness-dependent resistivity, mobility and carrier concentration of the IMO heteroepitaxial structure are shown in Fig. 2b. The conductivity of the IMO/AZO/mica structure obviously increased as the thickness increased, which was related to an increase in the electron mobility for thicknesses from 100 to 400 nm. The resistivity was $2.62 \times 10^{-4}\,\Omega$ cm and decreased to $1.17 \times 10^{-4}\,\Omega$ cm as the thickness of IMO increased from 100 to 400 nm. The electron mobility and carrier concentration were $56.5\,cm^2\,V^{-1}\,s^{-1}$ and $4.90 \times 10^{20}\,cm^{-3}$ for a 100 nm thickness and $88\,cm^2\,V^{-1}\,s^{-1}$ and $6.06 \times 10^{20}\,cm^{-3}$ for a 400 nm thickness, respectively. It was obvious that as the thickness of the IMO film increased, an increase in the crystallinity was obtained, which reduced the scattering of the carrier and showed increased transport behavior. A comparison was made between the IMO/AZO/mica heteroepitaxial structure in this study and the currently reported IMO thin films in Table 1. It is clear from the table that the heterostructure in this work showed a very low resistivity among all the IMO thin films due to both its relatively high-mobility and carrier concentration, which were related to the high crystallinity. Based on our results, IMO/AZO/mica heteroepitaxial structures have excellent performance and can play a potential key role in advanced electronics applications.

Since IMO has exceptional transport behavior and high optical transparency, it is critical to characterize the optical transparency of the IMO/AZO/mica structure and discuss its conductivity. A photograph of a 2-inch wafer with a 400 nm IMO on AZO/mica, as shown in the inset of Fig. 3a, directly illustrates the high optical transparency of the heteroepitaxial structure. The optical transmittance spectra of IMO heterostructures with various thicknesses are shown in Fig. 3a. The pure muscovite substrate had a high transmittance without absorption over the whole measured range. Above the muscovite substrate, the IMO/AZO/mica heterostructure showed an average visible transmittance of 81–83% with a thickness from 100 to 400 nm. The observed oscillation in the spectra was caused by interference effects. The transmittance of the heteroepitaxial structure in the visible range slightly decreased with increasing thickness. A figure of merit (Φ_{TC}), which is an important parameter, was used to identify and compare the performance of all transparent conducting elements. The value of Φ_{TC} was defined to be T^{10}/R_s (Ω^{-1}), where R_s is the sheet resistance and T is the average optical transmittance. Typically, a higher Φ_{TC} indicates an increased performance for transparent conducting films. The Φ_{TC} for the IMO/AZO/mica structure with various thicknesses, IMO films[17,20,21,23–34] and numerous TCO films on flexible substrates[14,35–44] are shown in Fig. 3b. The ultrahigh figure of merit values for the IMO/AZO/mica heteroepitaxial structure can be observed due to its excellent characteristics. A very high

Table 1 An overview of recent works on IMO thin films with their properties.

Technique	$T_{process}$ (°C)	Φ (10^{-3} Ω^{-1})	R_s (Ω/□)	T (%)	ρ (Ω cm)	μ (cm^2 V^{-1} s^{-1})	n (cm^{-3})	Mo doping	Thickness (nm)	Substrate
RF sputtering[a]	550	97.6	1.37	81.8	4.5×10^{-5}	109	1.3×10^{21}	4 wt%	300	Mica
PLD[23]	700	39.18	8.9	90	8.9×10^{-5}	138	4.7×10^{20}	2 at%	100	Quartz
AA-CVD[15]	450	31.29	1.8	75	1.2×10^{-4}	119	4.4×10^{20}	–	650	Glass
RTE[17]	350	21.47	5	80.0	1.8×10^{-4}	130	2.6×10^{20}	4 wt%	370	Glass
ARE[25]	300	18	26	93	6.5×10^{-4}	24	4.0×10^{20}	3 at%	250	Glass
AACVD[26]	450	13.3	2.1	69.9	1.4×10^{-4}	123	3.7×10^{20}	3.1 at%	670	Soda lime glass
Spray pyrolysis[24]	550	10.2	1.33	83	4.0×10^{-4}	148	1.0×10^{20}	0.5 at%	300	Glass
Mist-CVD[21]	600	7.04	8	75	4.4×10^{-4}	93	1.5×10^{20}	0.8 at%	550	Glass
Co-sputtering[27]	600	5.24	24.57	81.6	4.9×10^{-4}	40	2.5×10^{20}	–	200	Glass
Spray pyrolysis[28]	400	2.5	17.2	73	6.8×10^{-4}	90	1.0×10^{21}	0.5 at%	525	Glass
RF sputtering[20]	300	1.51	71	80	3.55×10^{-4}	41.56	4.2×10^{20}	2.36 wt%	50	Glass
RF sputtering[22]	550	1.14	49.48	75.0	4.95×10^{-4}	27	4.7×10^{20}	2.0 wt%	100	Soda lime glass

[a]This work.

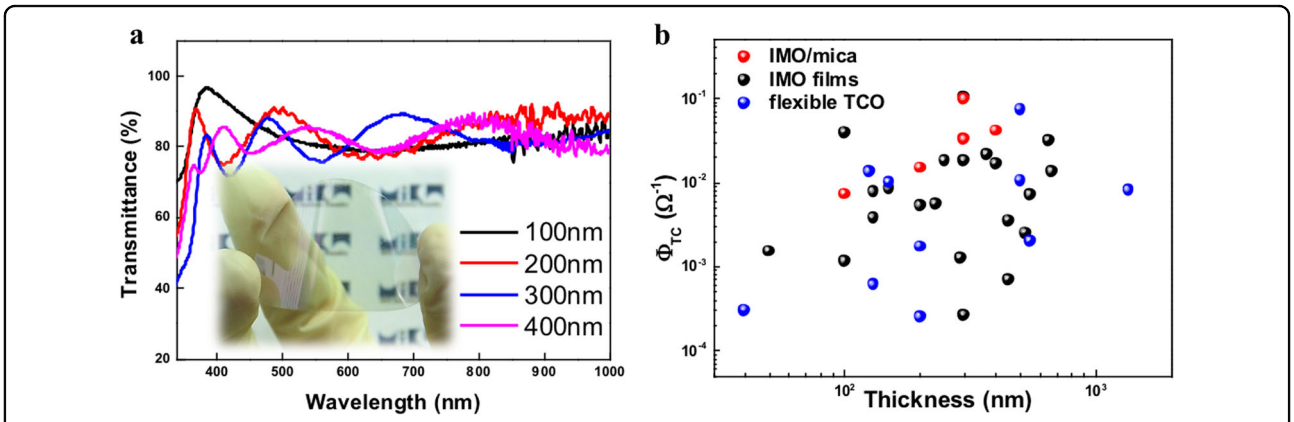

Fig. 3 Transparency of the IMO/AZO/mica heterostructure. a Optical transmittance spectra of the IMO heteroepitaxial structure with various thicknesses. **b** The figure of merit as a function of thickness of IMO/AZO/mica (red), IMO films[17,20,21,23–34] (black), and different TCO films on a flexible substrate[14,35–44] (blue).

Φ_{TC} value of 0.0976 Ω^{-1} was achieved for the best IMO/AZO/mica heterostructure, which exhibited high mobility (109 cm^2 V^{-1} s^{-1}), low sheet resistance (1.37 Ω □$^{-1}$) and high optical transmittance (81.8%). As a result, the transparent conducting IMO/AZO/mica heterostructure exhibited remarkable performance beyond that for all reported flexible TCO films.

Furthermore, to extend the practical application of this IMO/AZO/mica heterostructure with mechanical flexibility, a range of cycling tests were carried out. The operational stability and mechanical durability of the flexible IMO/AZO/mica heteroepitaxial structures were tested under both compressive (flex-in) and tensile (flex-out) bending states, as shown in the insets in Fig. 4a, b. Figure 4a, b shows that the resistance of the 300-nm thick heterostructure remained nearly constant with a bending radius down to 3.5 mm under both compressive and tensile deformations, respectively. Heterostructures with thicknesses of 100 and 200 nm also exhibited a steady conductivity with bending radii down to 5 mm. Thus, IMO heteroepitaxial structures were robust against mechanical constraints for flexible device applications. Due to only weak van der Waals interactions between the IMO/AZO and muscovite and small film-to-substrate

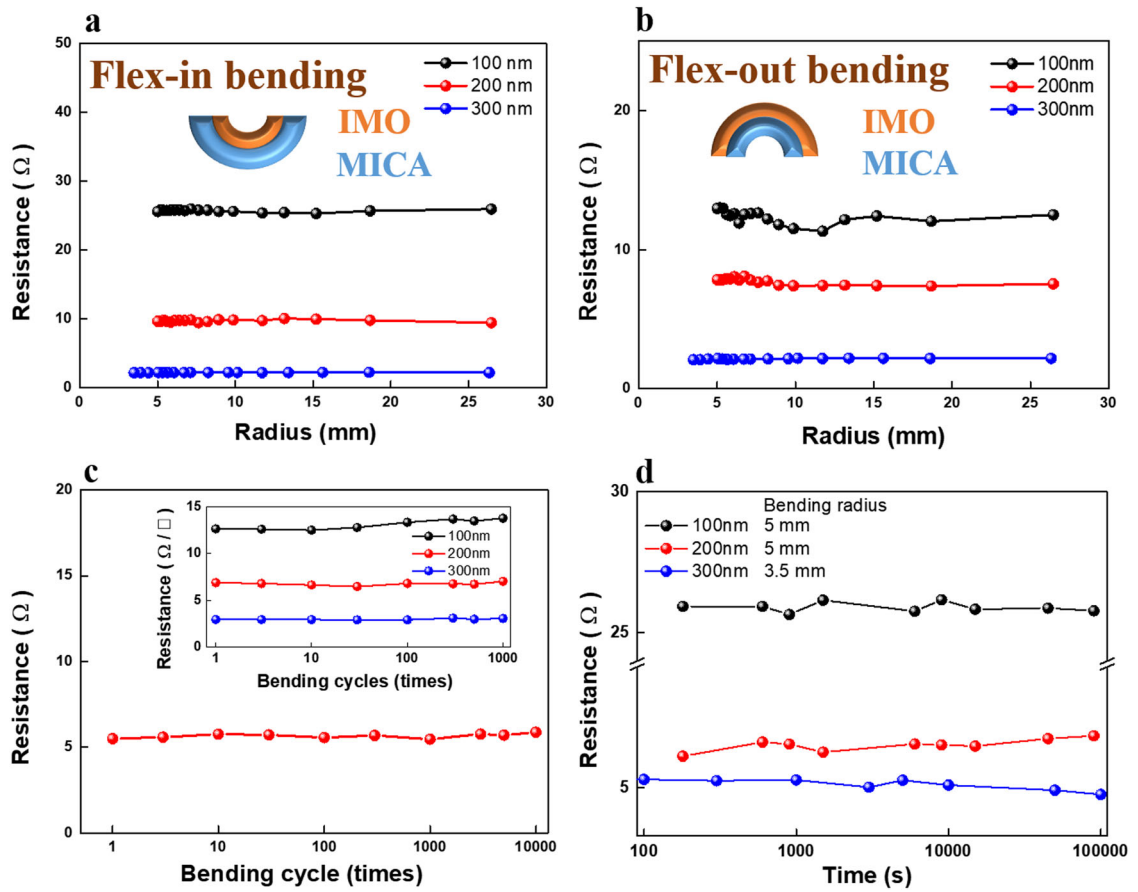

Fig. 4 Electrical properties under mechanical bending. a, **b** Resistance of the IMO heterostructure as a function of bending radius under **a** flex-in and **b** flex-out conditions with various thicknesses. **c**, **d** The stability and durability of the heteroepitaxial structure as a function of **c** repeated bending cycles and **d** continued bending time. The insets show the resistance as a function of bending cycles for various thicknesses.

thickness ratio, it was clear that the strain applied by bending was not enough to affect the behaviors of the IMO. In addition, the fluctuation of the resistance for the IMO heterostructures with the same thickness in Fig. 4 was caused by the difference in the contact resistance and displacement of the contact, since the contact was remade when the sample switched between different bending states. The stability of the heterostructure was investigated by measuring the conducting behavior as a function of bending cycles and time in flex-in mode. The resistance of the IMO/AZO/mica structure was steady and increased ~7% after 10,000 bending cycles under a bending radius of 3.5 mm, as shown in Fig. 4c. The thickness-dependent conduction stability of the IMO heterostructures is shown in the inset of Fig. 4c, which showed little change in the resistance of the heteroepitaxial structure, especially at a thickness of 300 nm after 10,000 bending cycles under a bending radius of 3.5 mm. Figure 4d shows that the conduction behavior of the IMO heterostructure was stable under compressive bending for a long duration under room-temperature environmental conditions. Moreover, the durability of the IMO/AZO/mica structure was studied under both mechanical bending and electrical bias. To simulate a practical condition, we applied a steady voltage of 5 V to the heterostructure with a bending radius of 3.5 mm, and an additional resistor was added into the circuit to control the current (0.2 A) flow through the IMO/AZO/mica heterostructure. A negligible change (<3%) was observed after one month. This indicates long-term conducting stability of the heterostructure under mechanical bending and electrical bias. Table 2 exhibits the conducting features of the flexible IMO/AZO/mica heteroepitaxial structure and recently reported TCOs on flexible substrates. Obviously, the heterostructure in this work had the best conducting performance among all flexible TCOs with a mobility over 100 $cm^2 V^{-1} s^{-1}$. Therefore, it is evident that the transparent flexible conducting IMO/AZO/mica heterostructure exhibited a performance superior to that of other flexible TCOs and an excellent stability, which are highly beneficial for advanced flexible optoelectronic applications.

Table 2 Summary of the flexible TCOs reported.

	Technique	Φ (10^{-3} Ω^{-1})	R_s (Ω/□)	T (%)	ρ (Ω cm)	μ (cm^2 V^{-1} s^{-1})	n (cm^{-3})	Thickness (nm)	Substrate
IMO[a]	RF sputter	97.6	1.37	81.8	4.5×10^{-5}	109	1.3×10^{21}	300	Mica
ITO[14]	PLD	10	10.74	80	5.0×10^{-5}	50	2.5×10^{21}	150	Mica
Ti-ZnO[35]	ALD	0.3	500	82.5	2.0×10^{-3}	19.5	1.5×10^{20}	40	Willow glass
AZO[36]	RF sputter	74	7.1	93.7	3.5×10^{-4}	17.5	1.0×10^{21}	500	Willow glass
IZO[37]	RF sputter	0.6	223	82	2.9×10^{-3}	27.7	1.3×10^{20}	130	PEN
GZO[38]	RF sputter	1.73	108.24	89.1	3.0×10^{-3}	8.5	6.0×10^{19}	200	PEN
AZO[39]	RF sputter	10.5	7	77	3.5×10^{-4}	22	8.0×10^{20}	500	PEN
ATO/Ag[40]	Co-sputtering	21.7	6.11	81.7	2.4×10^{-5}	16	1.5×10^{22}	40	PEN
ZnO[41]	CAPD	2.0	96.4	85	5.2×10^{-3}	18	1.3×10^{20}	550	PET
ZnO:B[42]	MOCVD	8.0	13.44	80	1.8×10^{-3}	22.2	2.1×10^{16}	1350	PET

[a]This work.

Conclusion

In conclusion, a high-quality transparent flexible conducting IMO/AZO/mica heteroepitaxial structure was successfully fabricated with a mobility larger than $100\,cm^2\,V^{-1}\,s^{-1}$, very high figure of merit ($0.0976\,\Omega^{-1}$), relatively low resistivity ($\sim 4.5 \times 10^{-5}\,\Omega\,cm$), high carrier concentration ($1.3 \times 10^{21}\,cm^{-3}$), and high optical transmittance (81.8%) at room temperature. In addition, this heterostructure retained the excellent performance with good flexibility. This study demonstrated an extraordinary achievement and can accelerate next-generation transparent flexible optoelectronics.

Acknowledgements

This work was supported by the Ministry of Science and Technology, Taiwan (Grant Nos. MOST 106-2119-M-009-011-MY3, 108-2628-E-009-006), Academia Sinica, Taiwan (AS-iMATE-107-11), and the Center for Emergent Functional Matter Science of National Chiao Tung University from The Featured Areas Research Center Program within the framework of the Higher Education Sprout Project by the Ministry of Education (MOE) in Taiwan.

Conflict of interest

The authors declare that they have no conflict of interest.

Supplementary information is available for this paper at https://doi.org/10.1038/s41427-020-00251-2.

Received: 11 January 2020 Revised: 24 August 2020 Accepted: 2 September 2020.
Published online: 23 October 2020

References

1. Lewis, B. G. & Paine, D. C. Applications and processing of transparent conducting oxides. *MRS Bull.* **25**, 22 (2000).
2. Dixon, S. C., Scanlon, D. O., Carmalta, C. J. & Parkin, I. P. n-type doped transparent conducting binary oxides: an overview. *J. Mater. Chem. C.* **4**, 6946–6961 (2016).
3. Stadler, A. Transparent conducting oxides—an up-to-date overview. *Materials (Basel)* **5**, 661–683 (2012).
4. Liu, H. et al. Transparent conducting oxides for electrode applications in light emitting and absorbing devices. *Superlattices Microst.* **48**, 458–484 (2010).
5. Calnan, S. & Tiwari, A. N. High mobility transparent conducting oxides for thin film solar cells. *Thin Solid Films* **518**, 1839–1849 (2010).
6. Babicheva, V. E., Boltasseva, A. & Lavrinenko, A. V. Transparent conducting oxides for electro-optical plasmonic modulators. *Nanophotonics* **4**, 165–185 (2015).
7. Hamers, R. J. Flexible electronic futures. *Nature* **412**, 489–490 (2001).
8. Liu, Y., Pharr, M. & Salvatore, G. A. Lab-on-skin: a review of flexible and stretchable electronics for wearable health monitoring. *ACS Nano* **11**, 9614–9635 (2017).
9. Zhang, L., Xiao, W., Wu, W. & Liu, B. Research progress on flexible oxide-based thin film transistors. *Appl. Sci.* **9**, 773 (2019).
10. Hosono, H. Recent progress in transparent oxide semiconductors: materials and device application. *Thin Solid Films* **515**, 6000–6014 (2007).
11. Yasuhara, R., Murai, S., Fujita, K. & Tanaka, K. Atomically smooth and single crystalline indium tin oxide thin film with low optical loss. *Phys. Status Solidi C.* **9**, 2533–2536 (2012).
12. Saberin, J. R. & Furse, C. Challenges with optically transparent patch antennas. *IEEE Antennas Propag. Mag.* **54**, 10–16 (2012).
13. Choi, K.-H. et al. Characteristics of flexible indium tin oxide electrode grown by continuous roll-to-roll sputtering process for flexible organic solar cells. *Sol. Energy Mater. Sol. Cells* **93**, 1248–1255 (2009).
14. Bitla, Y. et al. Oxide heteroepitaxy for flexible optoelectronics. *ACS Appl. Mater. Interfaces* **8**, 32401–32407 (2016).
15. Bhachu, D. S. et al. The origin of high mobility in molybdenum doped indium oxide. *Chem. Mater.* **27**, 2788–2796 (2015).
16. Elangovan, E. et al. Thin-film transistors based on indium molybdenum oxide semiconductor layers sputtered at room temperature. *IEEE Electron Device Lett.* **32**, 10 (2011).
17. Meng, Y. et al. A new transparent conductive thin film In_2O_3:Mo. *Thin Solid Films* **394**, 219–223 (2001).
18. Wu, P.-C. & Chu, Y.-H. Development of oxide heteroepitaxy for soft technology. *J. Mater. Chem. C.* **6**, 6102 (2018).
19. Chu, Y.-H. Van der Waals oxide heteroepitaxy. *npj Quantum Mater.* **2**, 67 (2017).
20. Chang, H.-J., Chen, W.-F., Huang, K.-M., Ho, C.-L. & Wu, M.-C. Deposition of transparent indium molybdenum oxide thin films and the application for organic solar cells. *Jpn. J. Appl. Phys.* **51**, 02BK02 (2012).
21. Yamada, N. et al. High-through put optimization of near-infrared-transparent Mo-doped In_2O_3 thin films with high conductivity by combined use of atmospheric-pressure mist chemical-vapor deposition and sputtering. *Thin Solid Films* **626**, 46–54 (2017).

22. DeAngelis, A. D. et al. Temperature-resistant high-infrared transmittance indium molybdenum oxide thin films as an intermediate window layer for multi-junction photovoltaics. *Sol. Energy Mater. Sol. Cells* **127**, 174–178 (2014).
23. Gupta, R. K., Ghosh, K., Mishra, S. R. & Kahol, P. K. Structural, optical and electrical characterization of highly conducting Mo-doped In_2O_3 thin films. *Appl. Surf. Sci.* **254**, 4018–4023 (2008).
24. Parthiban, S. et al. Investigations on high visible to near infrared transparent and high mobility Mo doped In_2O_3 thin films prepared by spray pyrolysis technique. *Sol. Energy Mater. Sol. Cells* **94**, 406–412 (2010).
25. Kaleemulla, S., Sivasankar Reddy, A., Uthanna, S. & Sreedhara Reddy, P. Room temperature photoluminescence property of Mo-doped In_2O_3 thin films. *Curr. Appl. Phys.* **10**, 386–390 (2010).
26. Swallow, J. E. N. et al. Resonant doping for high mobility transparent conductors: the case of Mo-doped In_2O_3. *Mater. Horiz.* **7**, 236–243 (2020).
27. Shin, Y.-H., Kim, H.-K. & Na, S.-I. Effect of MoO_3 doping power on the electrical, optical, and structural properties of MoO_3-doped In_2O_3 anodes for organic solar cells. *J. Vac. Sci. Technol. A* **30**, 061507 (2012).
28. Parthiban, S. et al. Structural, optical and electrical properties of indium–molybdenum oxide thin films prepared by spray pyrolysis. *Phys. Status Solidi A* **207**, 1554–1557 (2010).
29. Parthiban, S. et al. Effect of Li^{3+} heavy ion irradiation on the Mo doped In_2O_3 thin films prepared by spray pyrolysis technique. *J. Phys. D Appl. Phys.* **44**, 085404 (2011).
30. Elangovan, E. et al. Effect of annealing on molybdenum doped indium oxide thin films RF sputtered at room temperature. *Vacuum* **82**, 1489–1494 (2008).
31. Gokulakrishnan, V. et al. Investigation of O^{7+} swift heavy ion irradiation on molybdenum doped indium oxide thin films. *Radiat. Phys. Chem.* **81**, 589–593 (2012).
32. Sun, S.-Y., Huang, J.-L. & Lii, D.-F. Properties of indium molybdenum oxide films fabricated via high-density plasma evaporation at room temperature. *J. Mater. Res.* **20**, 247–255 (2005).
33. Parthiban, S. et al. High near-infrared transparent molybdenum-doped indium oxide thin films for nanocrystalline silicon solar cell applications. *Sol. Energy Mater. Sol. Cells* **93**, 92–97 (2009).
34. Elangovan, E., Martins, R. & Fortunato, E. Effect of base and oxygen partial pressures on the electrical and optical properties of indium molybdenum oxide thin films. *Thin Solid Films* **515**, 8549–8552 (2007).
35. Lee, W.-J. et al. Optimization of bending durability of Ti-ZnO thin films on flexible glass substrates with highly enhanced optoelectronic characteristics by atomic layer deposition. *Jpn. J. Appl. Phys.* **58**, 075501 (2019).
36. Ghosh, S. et al. Study on AZO coated flexible glass as TCO substrate. In *IEEE 43rd Photovoltaic Specialists Conference* (IEEE, 2016).
37. Silva-Lopez, H. E., Marcelino, B. S., Guillen-Cervantes, A., Zelaya-Angel, O. & Ramirez-Bon, R. Physical properties of sputtered indium-doped ZnO films deposited on flexible transparent substrates. *Mater. Res.* **21**, e20180224 (2018).
38. Chin, H.-S., Chao, L.-S. & Wu, C.-C. Crystal, optical, and electrical characteristics of transparent conducting gallium-doped zinc oxide films deposited on flexible polyethylene naphthalate substrates using radio frequency magnetron sputtering. *Mater. Res. Bull.* **79**, 90–96 (2016).
39. Hamrit, S. et al. The effect of thickness on the physico-chemical properties of nanostructured ZnO:Al TCO thin films deposited on flexible PEN substrates by RF-magnetron sputtering from a nanopowder target. *Ceram. Int.* **42**, 16212–16219 (2016).
40. Yu, S. et al. Transparent conductive Sb-doped SnO_2/Ag multilayer films fabricated by magnetron sputtering for flexible electronics. *Acta Mater.* **61**, 5429–5436 (2013).
41. Yang, R.-Y. et al. Low-temperature deposited ZnO thin films on the flexible substrate by cathodic vacuum arc technology. *Appl. Surf. Sci.* **257**, 7119–7122 (2011).
42. Chen, X.-I. et al. Textured surface boron-doped ZnO transparent conductive oxides on polyethylene terephthalate substrates for Si-based thin film solar cells. *Thin Solid Films* **520**, 1263–1267 (2011).
43. Wu, J.-L. et al. Effects of ZnO buffer layer on characteristics of ZnO:Ga films grown on flexible substrates: investigation of surface energy, electrical, optical, and structural properties. *ECS J. Solid State Sci. Technol.* **2**, 115–119 (2013).
44. Shin, S. W. et al. Development of flexible Mg and Ga co-doped ZnO thin films with wide band gap energy and transparent conductive characteristics. *J. Alloy. Compd.* **585**, 608–613 (2014).